## Title

# Advanced Interferometry with 3-D Structured Illumination Reveals the Surface Fine Structure of Complex Biospecimens


## Authors

Takahisa Matsuzaki,[1,2*] Ryuzo Kawamura,[3] Akihisa Yamamoto,[4] Hozumi Takahashi,[1] Mai Fujii,[3] Shodai Togo,[3] Yosuke Yoneyama[5], Fumihiko Hakuno[5], Shin-Ichiro Takahashi[6], Masami Suganuma,[7] Seiichiro Nakabayashi,[7] Shivani Sharma,[8] James K. Gimzewski,[8,9,10] Hiroshi Y. Yoshikawa[1*]

## Affiliation

[1]Department of Applied Physics, Graduate School of Engineering, Osaka University, 2-1, Yamadaoka, Suita 565-0871, Japan.
[2]Center for Future Innovation, Graduate School of Engineering, Osaka University, 2-1, Yamadaoka, Suita, Osaka 565-0871, Japan.
[3]Department of Chemistry, Saitama University, 255 Shimo-Okubo, Sakura-Ku, Saitama 338-8570, Japan.
[4]Center for Integrative Medicine and Physics, Institute for Advanced Study, Kyoto University, Kyoto 606-8501, Japan
[5]Institute of Research, Tokyo Medical and Dental University (TMDU), 1-5-45 Yushima bunkyo-Ku, Tokyo 113-8510, Japan
[6]Departments of Animal Sciences and Applied Biological Chemistry, Graduate School of Agriculture and Life Sciences, The University of Tokyo, Bunkyo-Ku, Tokyo 113-8657, Japan.
[7]Division of Strategic Research and Development, Graduate School of Science and Engineering, Saitama University, 255 Shimo-Okubo, Sakura-Ku, Saitama 338-8570, Japan.
[8]California NanoSystems Institute, University of California, Los Angeles, Los Angeles, CA, United States.
[9]Department of Chemistry and Biochemistry, University of California, Los Angeles, Los Angeles, CA, United States.
[10]WPI Center for Materials Nanoarchitectonics (MANA), National Institute for Materials Science (NIMS), Tsukuba, Japan

## Corresponding

*Double corresponding authors
・Takahisa Matsuzaki
mail: matsuzaki@ap.eng.osaka-u.ac.jp Tel: +81-6-6879-7838
・Hiroshi Y Yoshikawa
mail: hiroshi@ap.eng.osaka-u.ac.jp Tel: +81-6-6879-7838


## Notes

The authors declare no competing financial interest.


## Abstract

Interference reflection microscopy (IRM) is a powerful, label-free, technique to visualize the surface structure of biospecimens. However, stray light outside a focal plane, obscures the surface fine structures beyond the diffraction limit ($d_{xy}$ ~ 200 nm). Here, we developed an advanced interferometry approach to visualize the surface fine structure of complex biospecimens, ranging from protein assemblies to single cells. Compared to 2D, our unique 3-D structure illumination introduced to IRM, enabled successful visualization of fine structures and the dynamics of protein crystal growth under lateral ($d_{x\text{-}y}$ ~110 nm) and axial ($d_{x\text{-}z}$ ≤ 5 nm) resolutions; and dynamical adhesion of microtubule fiber networks with lateral resolution ($d_{x\text{-}y}$ ~120 nm), ten times greater than unstructured IRM ($d_{x\text{-}y}$ ~1000 nm). Simultaneous reflection/fluorescence imaging provides new physical fingerprints for studying complex biospecimens and biological processes such as myogenic differentiation; and highlights the potential use of advanced interferometry to study key nanostructures of complex biospecimens.

## TOC graphics

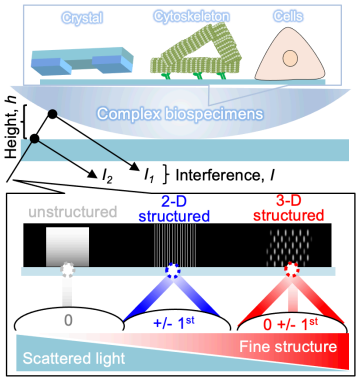



## Keywords

Interference reflection microscopy, Structured illumination, Crystal growth, Microtubule fiber network, Cell Adhesion.


## Main text

Interference reflection microscopy (IRM), is one of the leading, label-free, techniques for visualizing nanoscopic axial topography[1-3] using the interference between light reflected from the surface of the biospecimens ($I_1$) and substrate ($I_2$) (**Figure 1A**). Due to the interference intensity ($I$) in monochromatic IRM images depending on height ($h$), thus the greatest advantage of IRM is to evaluate $h$ at the resolution of the sub-nm scale in a label-free manner[3]. However, conventional IRM setups adopt homogenous illumination light[4]; where stray light from the internal structure of complex biospecimens, obscures the surface fine structures beyond the diffraction limit ($d_{xy}$ ~ 200 nm).

Alternatively, various super-resolution "fluorescence" microscopies, such as stimulated emission depletion microscopy (STED), photoactivated localization microscopy (PALM), and stochastic optical reconstruction microscopy (STORM), structured illumination microscopy (SIM) have been well-developed[5, 6]. Among those techniques that rely on specialized nonlinear properties of fluorophores[7, 8], SIM achieved lateral super-resolution via non-restrictions on fluorophore types using only its instrumental aspect (*i.e.,* Moiré fringes). Moreover, for obtaining fluorescence images of complex biospecimens such as cells, optical sectioning via 3-D structured illumination efficiently eliminates stray light outside a focal plane (*e.g.,* organelles, cytoskeleton, etc.) that obscure fluorescence signals[9]. However, the axial resolution of conventional SIM is approximately in the range of several hundred nanometers, which is insufficient for imaging surface nanostructures of complex biospecimens.

To overcome long-standing limitations of IRM to visualize complex biospecimens with sufficient lateral resolution, we combined such optical sectioning concepts of 3-D structured illumination with IRM (*i.e.,* 3-D SIM-IRM). We introduced structured illumination as a light source to the IRM optical setup (**Figure 1B bottom**, further details: **SI method**), and prepared three illumination patterns using diffraction grating[7, 8] (**Figure 1B top**): unstructured illumination ($0^{th}$-order diffraction light), 2-D structured illumination on the lateral plane (interference among $1^{st}$-order diffraction light), and 3-D structured illumination along the optical axis (interference between $1^{st}$- and $0^{th}$-order diffraction light). Based on the optical setups, in this work, we systematically compared the image contrast of biospecimens between unstructured and 2-D/3-D structured illuminations. Further, we visualized the molecular organization and dynamics of complex biospecimens, such as protein molecular assemblies (crystals, cytoskeleton) and single cells (**Figure 1A**).

Before visualizing complex biospecimens, we first systematically verified the IRM image contrast of a polystyrene bead on a glass substrate under un-/2-D/3-D structured illumination (**Figure 1C**). Here, the Moiré pattern (real space) for interference images was also visible, as in the case of fluorescence images (**Figure S1A, S1B, magnification**), leading to the success of image reconstruction for IRM images. In contrast to IRM images under unstructured illumination producing untargeted interference (*i.e.,* speckles), Newton's ring-like fringes in IRM images were clearly observed under 2-D and 3-D structured illumination. **Figure 1D** shows intensity profiles according to the dotted line in **Figure 1C**. The result also supports that optical sectioning via 3-D structured illuminations eliminated scattered

light from untargeted planes, thereby enhancing the contrast with low noises. Second, we verified the qualitative lateral resolution of obtained IRM images via a fast Fourier transform (FFT) analysis for **Figure 1C**. FFT space images showed a flower-like structure in frequency space (**Figure 1E**) which was also seen in the case of our fluorescence SIM data (**Figure S1B, bottom**) and other group's ones[10] implying the lateral resolution reaching the super-resolution regime. We also analyzed the FFT power spectrum (**Figure 1F**) of the intensity profile along the dotted line in **Figure 1E**. In the case of unstructured illumination used, FFT power exponentially decays to reach a plateau, which is the potential noise level (mean power = 90 ± 7). It should be noted that the FFT power under unstructured illumination does not be beyond the diffraction limit ($f$ = 5 μm$^{-1}$, corresponding to $d_{xy}$ ~ 200 nm) which is defined by the abbe equation. In contrast, FFT power under 3-D structured illumination is above noise level till the $f$ = 8.5 μm$^{-1}$ ($d_{xy}$ = 118 nm) which is surely beyond the diffraction limit. Thus, these FFT power spectrum analyses suggest 3-D SIM-IRM reaches the super-resolution regime. It should be noted that the FFT power of typical fluorescence SIM[10] also reaches the background noise at a comparable frequency of 3-D SIM-IRM (data not shown). To evaluate whether IRM's theoretical bases for height reconstruction remain in 3-D SIM-IRM, we reconstructed height profiles according to the dotted line in **Figure 1C**. Here, interference intensity generally can be written as **Eq. (1)**:

$$I = I_1 + I_2 + 2\sqrt{I_1 I_2}\cos\left(4\pi n h/\lambda + \pi\right)$$

and previous works derive practical equations to convert $I$ to $h$ assuming quasi-normal incidence[3] as **Eq. (2)**:

$$\frac{2I-(I_{\max}+I_{\min})}{-(I_{\max}+I_{\min})} = \cos\left(\frac{4\pi n}{\lambda}h\right)$$

where $I$ is the measured intensity, $I_{max}$ and $I_{min}$ are the maximum and minimum intensities, respectively. $\lambda$ is the wavelength of light, $n$ is the refractive index of the medium (~1.333). Reconstructed height profiles under unstructured illumination led to severe rough surfaces (**Figure 1G**) which is influenced by the untargeted speckle pattern in **Figure 1D**. In contrast, the reconstructed height profile of the polystyrene bead under 3-D structured illumination is in good agreement with its predicted height profile ($\Phi$ = 100 μm) up to 0.15 μm from the surface. It should be noted that the most crucial point is to visualize the newton fringes with enhanced contrast, and the success in reconstructing height profiles of beads. Based on these results, we revealed that 3-D structured illumination eliminated scattered light from untargeted planes, thereby reaching a lateral super-resolution regime that was validated in FFT power spectrum analysis. We also revealed that IRM's theoretical bases for height reconstruction can be valid for SIM-IRM.

As a first trial to visualize the fine structure of "actual" biospecimens beyond the diffraction limit ($d_{xy}$ ~ 200 nm), elementary steps on the surface of protein crystals were monitored, which also can provide deeper insights into the fundamental mechanism of crystal growth[11-13]. The crystals of hen egg-white lysozyme (HEWL), widely used to study the growth mechanism of a protein crystal, were placed on a glass substrate using beads (diameter ~ 100 nm) as spacers (**Figure 2A**, sample preparation: **SI method**). 2-D island-like etch pits[14, 15] of dissolving (110) surface of HEWL crystals was visualized using 2-D/3-D structured illumination, whereas there was less contrast of pits with speckles using unstructured illumination (**Figure 2B**). Visible dark spots under the 2-D/3-D structured illumination are spacer beads (yellow arrowhead). Furthermore, not unstructured but 2-D/3-D structured illumination visualized multiple etch pits (**Figure 2B right**) highlighting the impact of the optical sectioning effect of 2-D/3-D SIM-IRM on crystal surface visualization. Interestingly, there were different interference signals of dissociating crystal surface under 3-D structured illumination (**Figure 2C**); thus we reconstructed the corresponding height image using **Eq. (2)**. Here, $I_{max}$ was carefully determined not from the crystal-solution interface but from the crystal-substrate interface (**Figure S2A, S2B**) as like our previous studies[16, 17]. Height profiles across the pits (red arrow) exhibit a height of $h$ ~ 5 nm, which is in good agreement with that of the elementary step of HEWL crystals[14, 15]. In addition, height profiles across the other pits showed multiple layers of the elementary step of HEWL crystals[14, 15] (blue arrow: $h$ ~ 20 nm (4 layers), red arrow: $h$ ~ 40 nm (8 layers), suggesting the presence of a spatial distribution of impurities and defect on the crystal surface (**Figure 2D**). Furthermore, 3-D SIM-IRM sensitively detected wide varieties of nano-structures during the dissociation of protein crystals (**movie S1.avi**). For instance, 2D-like islands were clearly detected (asterisk, **Figure 2E**) and the radial expansions fussed with each other. Topological profiles across both islands indicated the 2 layers of proteins ($t$ = 0 s, z ~ 10 nm, **Figure 2F**) leading to the formation of fine pits (circle, $t$ = 60 s, $xy$ ~ 100 nm, $z$ ~ 2 nm).

In the other spots after step fusions, multistep-like structures were formed "inside" etch pits (rectangle, **Figure S2C, S2D**, *xy* ~ 130 nm, *z* ~ 1 nm). These results clearly indicate that 3-D structured illumination enhances the contrast in IRM images for crystal growth, leading to visualizing fine structure beyond the diffraction limit ($d_{xy}$ ~ 200 nm). In addition, the evaluation of morphological changes inside the etch pits is also crucial in unveiling the mechanism of various crystal dissociation[18]. Such different nano-scale dissociation dynamics of proteins also provide physical insights into the spatial distribution of impurities and defects. We succeeded in dynamical imaging (0.5 flames/sec) for dissociating crystals; further high-speed imaging will provide deeper physical insight into the surface dynamics of biospecimens, where the rotary speed of diffraction gratings limits the temporal resolution. Interferometric scattering microscopy (iSCAT) combined with a spinning disk succeeded in visualizing the high-speed dynamics of nanoparticles inside cells [19]. Even though the iSCAT did not focus on the surface topological profiles, such a fundamental solution combined with high-speed rotating grating will improve the fundamental flame ratio. Thus, we highlight the advantage of our 3-D SIM-IRM with fine lateral and axial resolution in a label-free manner, while observations with fluorescence labeling and scanning probes potentially disturb the native surface and environmental properties during crystal growth [20].

Next, we verified the impact of 3-D SIM-IRM imaging on complex biospecimens (*i.e.,* three-dimensional networks of microtubule fibers). The motor proteins (kinesin) functionalized on a glass substrate drive the motion of the deposited microtubule fiber networks in the presence of chemical energy (adenosine triphosphate, ATP) (**Figure 3A,** sample preparation: **SI methods**). This is regarded as an *in vitro* complex model of the cytoskeleton and protein-based actuators[21]. Despite the fluorescence imaging identifying the presence of fibers near the glass substrate, IRM under un-/ 2-D structured illumination could not visualize the adhesion of microtubule fiber networks (**Figure 3B**). In contrast, the 3-D structured illumination facilitates the visualization of fiber-like structures in IRM and fluorescence microscope (FLM) images, even highlighting the impact of 3-D structured illumination to reduce the stray light from complex biospecimens. According to the intensity profiles across the fibers, 3-D SIM-IRM enabled the visualization of single fibers (~ 130 nm) beyond the diffraction limit ($d_{xy}$ ~ 200 nm, **Figure 3C**). To quantitatively confirm the enhancement of contrast of microtubule fibers via the introduction of structured illumination, the less-condensed microtubule fiber networks were imaged (**Figure S3A**). Introducing 3-D structured illumination enhanced the signal-to-noise (SN) ratio five times higher than unstructured illumination (**Figure S3B**). The contrast enhancement highlights the impact of not 2-D but 3-D structured illumination to reduce light scattering from internal fiber networks away from the glass substrate. The interference intensity of fibers corresponds to the fiber-substrate distance according to **Eq. (1)**; thus, we reconstructed height images from a 3-D SIM-IRM image (**Figure 3D left**). 3-D SIM-IRM clearly distinguished whether the fiber is closer (dark line, white arrowheads) or farther (white line, white asterisk) from the substrate, whereas fluorescence imaging under 3-D structured illumination (*i.e.,* 3-D SIM-FLM) identifies the presence of fibers near the substrate (**Figure 3D right**). It should be noted that there was no spatial correlation between reconstructed height and fluorescence intensity, which was different from the case of cells as described below (**Figure 4**). However, these results highlight the impact of simultaneous 3-D SIM-IRM/-FLM imaging leads to a quantitative assessment of the position of microtubule fibers along the optical axis. Next, we applied 3-D SIM-IRM to dynamic microtubule fiber networks with motor protein activated by ATP hydrolysis (**movie S2.avi**). 3-D SIM-FLM monitored the locomotion of a single microtubule fiber to meet the other fibers at $t$ = 148 s (**Figure 3E left**). However, the vertical positional relationship between fibers could not be obtained. In contrast, height reconstruction from 3-D SIM-IRM images using **Eq. (2)** indicated that locomoting fibers (red arrowhead, $t$ = 148 s) showed 2-4 times higher than the ones of tightly contacted to the substrate ($h \leqq 40$ nm, blue arrowheads) (**Figure 3E middle**). The results suggest that the locomoting fiber moved on top of the other fiber, and then showed loose contact during movement (**Figure 3E right**).Although conventional IRM studies evaluated the locomotion speed of isolated microtubule fibers[22, 23], highly crosslinked protein fiber networks increased the scattered light from internal fiber networks as seen in **Figure 3A**. Thus, we succeeded in visualizing such dynamical adhesion and its locomotion of the fiber network using fine lateral and axial information which conventional IRM and fluorescence imaging techniques cannot achieve.

To highlight the impact of simultaneous 3-D SIM-IRM/-FLM imaging for further complex biospecimens, we visualized the adhesion of a single myoblast cell (expressing fluorescent F-actin). In contrast to unstructured IRM/FLM only detected larger dark patch-like structures with blurred fluorescent fibers, 3-D SIM-IRM/-FLM visualized dark and mesh-like structures of the cell membrane which was supported by a fine network of fluorescent actin fibers (**Figure 4A**). Magnification of 3-D SIM-IRM in **Figure 4A** clearly detected fiber-like structures with dark contrast (**Figure 4B,** arrowhead) and the size (~ 130 nm) was beyond the diffraction limit ($d_{xy}$ ~ 200 nm) (**Figure 4C**). These results highlight the impact of optical sectioning via 3-D structured illumination, that efficiently eliminates stray light outside a focal plane (*e.g.,* organelles, cytoskeleton, etc.) that obscured fluorescence signals[9]. Next, we obtained a spatial correlation between the cell membrane and cytoskeleton structures in cell adhesion. Height reconstruction from 3-D SIM-IRM images using **Eq. (2)** enables us to classify cell adhesion area into tight contact area ($T$) and loose contact area (or unadhered area) ($L$) at the threshold of cell-substrate distance, $h$ ~ 40 nm (**Figure 4D left**), which is the comparable size to the extracellular domain of the cell adhesion molecules[17]. The structure of cell adhesion can be further classified according to the fluorescent level of F-actin (**Figure 4D right**), then adding text as a subscript to $T$ and $L$. As schematically illustrated in **Figure 4E (blue)**, $T_{High}$ region (tight contact with higher fluorescence (subscript)) suggests the formation of macromolecular assemblies (*i.e.,* focal complex) around the cell periphery via biological key-lock interaction, whereas $T_{Low}$ region (tight contact with lower fluorescence (subscript)) is attributed to direct contact via generic physical interaction [24] (*e.g.,* coulomb force and van der Waals forces, etc.). Also, as schematically illustrated in **Figure 4E (red)**, the $L_{High}$ region (loose contact with higher fluorescence) indicates repulsive interaction[24] with supporting cell morphology[25], whereas $L_{low}$ (loose contact with lower fluorescence) defines repulsive free membrane possibly via undulation interactions [24]. Together, these results clearly highlight the advantages of simultaneous 3-D SIM-IRM/-FLM imaging- with fine lateral and axial resolutions- for characterizing the local distribution of adhesion structures in single cells.

Finally, we applied simultaneous 3-D SIM-IRM/-FLM imaging to characterize the adhesion of multicellular myoblasts during myogenic differentiation. Cultivation of myoblasts at high cell densities activates cellular fusion (culturing procedures: **SI method**), resulting in differentiated myotubes with various biological characteristics (*e.g.,* multiple nuclei, expression of myogenin in **Figure S4A and S4B**). However, no previous report exists to answer whether classifying the local distribution of adhesion structures enables us to characterize the differentiation states from myoblasts to myotubes. Reconstructed height images from 3-D SIM-IRM images using **Eq. (2)** represent a monotonic decrease in height, indicating the adhesion transition from loose to tight contact according to the myogenic differentiation (**Figure 4F left**). 3-D SIM-FLM visualized a decrease in fluorescence intensity (Day 3), and an increase in the orientation of actin fibers (Day 6) (**Figure 4F right**). To visibly evaluate the local distribution of adhesion structures, we simultaneously plotted the height and fluorescence intensity of each pixel from 3-D SIM-IRM/-FLM images as density plots (**Figure 4G**). Adhesion of myoblasts (Day 0) showed loose contact with a broad expression of actin ($L_{High}$ and $L_{Low}$) via repulsive biophysical interaction. After induction of differentiation by serum starvation, the width of the distribution of dots became narrow due to a simultaneous decrease in height and fluorescence intensity (Day 3, myocytes). The peak changed to broad with shifting to the tight contact with higher fluorescence intensity ($T_{High}$) for myotubes (Day 6). These results indicate that simultaneous super-resolution imaging of cell membranes and cytoskeletal structures clearly detected the adhesion transition from loose to tight contact during myogenic differentiation (**Figure 4H, left and right**). Furthermore, we sensitively detected the intermediate differentiating stage with a narrow distribution of loose contact with low expression of actin (**Figure 4H, middle**). Based on the obtained results, simultaneous imaging of 3-D SIM-IRM and 3-D SIM-FLM may provide new, physical and biological fingerprints for myogenic differentiation. It should be noted that biological immunostaining only detected myotubes at a "fixed" time point (**Figure S4B**) demonstrating the potential applicability of our 3-D SIM-IRM/-FLM to unveil "dynamical" local complex mechanisms of the differentiation state triggered by cell-matrix adhesion.

In summary, we introduce the optical sectioning concept of structured illumination to the classical IRM, to obtain the surface visualization of complex biospecimens beyond the diffraction limit ($d_{xy}$ ~ 200 nm) (**Figure S5**). Lateral super-resolution was confirmed by the visualizing isolated fluorescent nanobeads (**Figure S6a-b**) and distinguishing adjacent fluorescent nanobeads (**Figure S6c-e**). Not

2-D but 3-D structure illumination introduced to IRM, successfully reduced stray light and visualized dynamical structures of protein crystal growth and microtubule fiber motion. Simultaneous imaging of 3-D SIM-IRM/-FLM enabled us to classify the adhesion of cells and provide new physical fingerprints for myogenic differentiation. Microscopic interference artifacts in the background (~ 2 μm peak to peak like **Figure 2B** and **Figure S3A**) do not interrupt the lateral super-resolution imaging. Still, future mathematical efforts should develop reconstruction algorithms that are specialized for our structured IRM. We foresee that advanced interferometry with 3-D structured illumination is expected to facilitate the discovery of critical fine structures of complex biospecimens from biomolecule assemblies to cells that regulate biological phenomena (*e.g.,* embryonic development and diseases).

## Associated contents

### ○Supporting Information

Supporting methods, figures (Figure S1-S6), and movies (Movie S1-S2) are available free of charge via the Internet at http://pubs.acs.org.


## Acknowledgments

This study was partly supported by grants received from the Japan Society for the Promotion of Science (JP21KK0195, JP 23K18563 to TM, J21H03790 to TM/HYY, JP22H00302, J22H05423, J23K18576, J20K21117 to HYY andJPJSCCA20210007 to SIT), Japan Science and Technology Agency (JPMJFR205N, Japan to TM), foundation (Nakatani Foundation to TM, Uehara Memorial Foundation to TM/HYY, Takeda Science Foundation to TM/HYY/MS/RK, Naito Foundation to HYY, Amada Foundation to HYY, and MEI Grant to HYY). TM expresses gratitude to Osaka University (Department of Research Promotion, Life-omics Research Division, Nikon Imaging Center) for their support and Haruka Matsumori (Nikon) for their technical assistance.


## Author contribution

TM and HYY conceived the study, designed/performed the experiments, collected/analyzed the data, and authored the manuscript. RK, YY, HT, MF, ST performed the experiments under TM and HYY's technical guidance and expertise. RK, AY, FH, SIT, MS, SN. SS, JKG authored and reviewed the manuscript.

## Declaration of interests

This study was conducted while Shivani Sharma was employed at the University of California, Los Angeles. The opinions expressed in this article are the author's own and do not reflect the view of the National Institutes of Health and Human Services or the United States government. The authors declare no competing financial interests.

## REFERENCES


(1) Curtis, A. The mechanism of adhesion of cells to glass: a study by interference reflection microscopy. *The Journal of cell biology* **1964**, *20* (2), 199-215.

(2) Rädler, J.; Sackmann, E. Imaging optical thicknesses and separation distances of phospholipid vesicles at solid surfaces. *Journal de Physique II* **1993**, *3* (5), 727-748.

(3) Limozin, L.; Sengupta, K. Quantitative reflection interference contrast microscopy (RICM) in soft matter and cell adhesion. *Chemphyschem* **2009**, *10* (16), 2752-2768.

(4) Verschueren, H. Interference reflection microscopy in cell biology: methodology and applications. *Journal of Cell Science* **1985**, *75* (1), 279-301.

(5) Schermelleh, L.; Heintzmann, R.; Leonhardt, H. A guide to super-resolution fluorescence microscopy. *J Cell Biol* **2010**, *190* (2), 165-175.

(6) Sigal, Y. M.; Zhou, R.; Zhuang, X. Visualizing and discovering cellular structures with super-resolution microscopy. *Science* **2018**, *361* (6405), 880-887.

(7) Gustafsson, M. G. Surpassing the lateral resolution limit by a factor of two using structured illumination microscopy. *Journal of microscopy* **2000**, *198* (2), 82-87.

(8) Heintzmann, R.; Huser, T. Super-Resolution Structured Illumination Microscopy. *Chem Rev* **2017**, *117* (23), 13890-13908.

(9) Li, X.; Wu, Y.; Su, Y.; Rey-Suarez, I.; Matthaeus, C.; Updegrove, T. B.; Wei, Z.; Zhang, L.; Sasaki, H.; Li, Y.; et al. Three-dimensional structured illumination microscopy with enhanced axial resolution. *Nature Biotechnology* **2023**.
(10) Demmerle, J.; Innocent, C.; North, A. J.; Ball, G.; Müller, M.; Miron, E.; Matsuda, A.; Dobbie, I. M.; Markaki, Y.; Schermelleh, L. Strategic and practical guidelines for successful structured illumination microscopy. *Nature Protocols* **2017**, *12* (5), 988-1010.
(11) Astier, J.-P.; Veesler, S. Using temperature to crystallize proteins: a mini-review. *Crystal Growth and Design* **2008**, *8* (12), 4215-4219.
(12) Nanev, C. Recent Insights into the Crystallization Process; Protein Crystal Nucleation and Growth Peculiarities; Processes in the Presence of Electric Fields. *Crystals* **2017**, *7* (10), 310.
(13) Gutiérrez-Quezada, A. E.; Arreguín-Espinosa, R.; Moreno, A. Protein Crystal Growth Methods. **2010**, 1583-1605.
(14) Sazaki, G.; Matsui, T.; Tsukamoto, K.; Usami, N.; Ujihara, T.; Fujiwara, K.; Nakajima, K. In situ observation of elementary growth steps on the surface of protein crystals by laser confocal microscopy. *Journal of Crystal Growth* **2004**, *262* (1-4), 536-542.
(15) Maruyama, M.; Kawahara, H.; Sazaki, G.; Maki, S.; Takahashi, Y.; Yoshikawa, H. Y.; Sugiyama, S.; Adachi, H.; Takano, K.; Matsumura, H.; et al. Effects of a Forced Solution Flow on the Step Advancement on {110} Faces of Tetragonal Lysozyme Crystals: Direct Visualization of Individual Steps under a Forced Solution Flow. *Crystal Growth & Design* **2012**, *12* (6), 2856-2863.
(16) Matsuzaki, T.; Sazaki, G.; Suganuma, M.; Watanabe, T.; Yamazaki, T.; Tanaka, M.; Nakabayashi, S.; Yoshikawa, H. Y. High Contrast Visualization of Cell-Hydrogel Contact by Advanced Interferometric Optical Microscopy. *J Phys Chem Lett* **2014**, *5* (1), 253-257.
(17) Matsuzaki, T.; Ito, K.; Masuda, K.; Kakinuma, E.; Sakamoto, R.; Iketaki, K.; Yamamoto, H.; Suganuma, M.; Kobayashi, N.; Nakabayashi, S.; et al. Quantitative Evaluation of Cancer Cell Adhesion to Self-Assembled Monolayer-Patterned Substrates by Reflection Interference Contrast Microscopy. *J Phys Chem B* **2016**, *120* (7), 1221-1227.
(18) Britt, D. W.; Hlady, V. In-situ atomic force microscope imaging of calcite etch pit morphology changes in undersaturated and 1-hydroxyethylidene-1, 1-diphosphonic acid poisoned solutions. *Langmuir* **1997**, *13* (7), 1873-1876.
(19) Hsiao, Y.-T.; Wu, T.-Y.; Wu, B.-K.; Chu, S.-W.; Hsieh, C.-L. Spinning disk interferometric scattering confocal microscopy captures millisecond timescale dynamics of living cells. *Optics Express* **2022**, *30* (25), 45233-45245.
(20) Dai, G.; Sazaki, G.; Matsui, T.; Tsukamoto, K.; Nakajima, K.; Kang, Q.; Hu, W. Gradual Immobilization Processes of Molecules during Transitions from Solute to Solid States. *Crystal Growth & Design* **2011**, *11* (1), 88-92.
(21) Kawamura, R.; Sano, K.-I.; Ijiro, K.; Osada, Y. Chemically cross-linked microtubule assembly shows enhanced dynamic motions on kinesins. *RSC Advances* **2014**, *4* (62), 32953-32959.
(22) Mahamdeh, M.; Simmert, S.; Luchniak, A.; Schaffer, E.; Howard, J. Label-free high-speed wide-field imaging of single microtubules using interference reflection microscopy. *J Microsc* **2018**, *272* (1), 60-66.
(23) Simmert, S.; Abdosamadi, M. K.; Hermsdorf, G.; Schaffer, E. LED-based interference-reflection microscopy combined with optical tweezers for quantitative three-dimensional microtubule imaging. *Opt Express* **2018**, *26* (11), 14499-14513.
(24) Sackmann, E.; Bruinsma, R. Cell adhesion as wetting transition? In *Physics of bio-molecules and cells. Physique des biomolécules et des cellules*, Springer, 2002; pp 285-309.
(25) Tsujita, K.; Takenawa, T.; Itoh, T. Feedback regulation between plasma membrane tension and membrane-bending proteins organizes cell polarity during leading edge formation. *Nat Cell Biol* **2015**, *17* (6), 749-758.
(26) Zwettler, F. U.; Reinhard, S.; Gambarotto, D.; Bell, T. D. M.; Hamel, V.; Guichard, P.; Sauer, M. Molecular resolution imaging by post-labeling expansion single-molecule localization microscopy (Ex-SMLM). *Nat Commun* **2020**, *11* (1), 3388.

## Figures

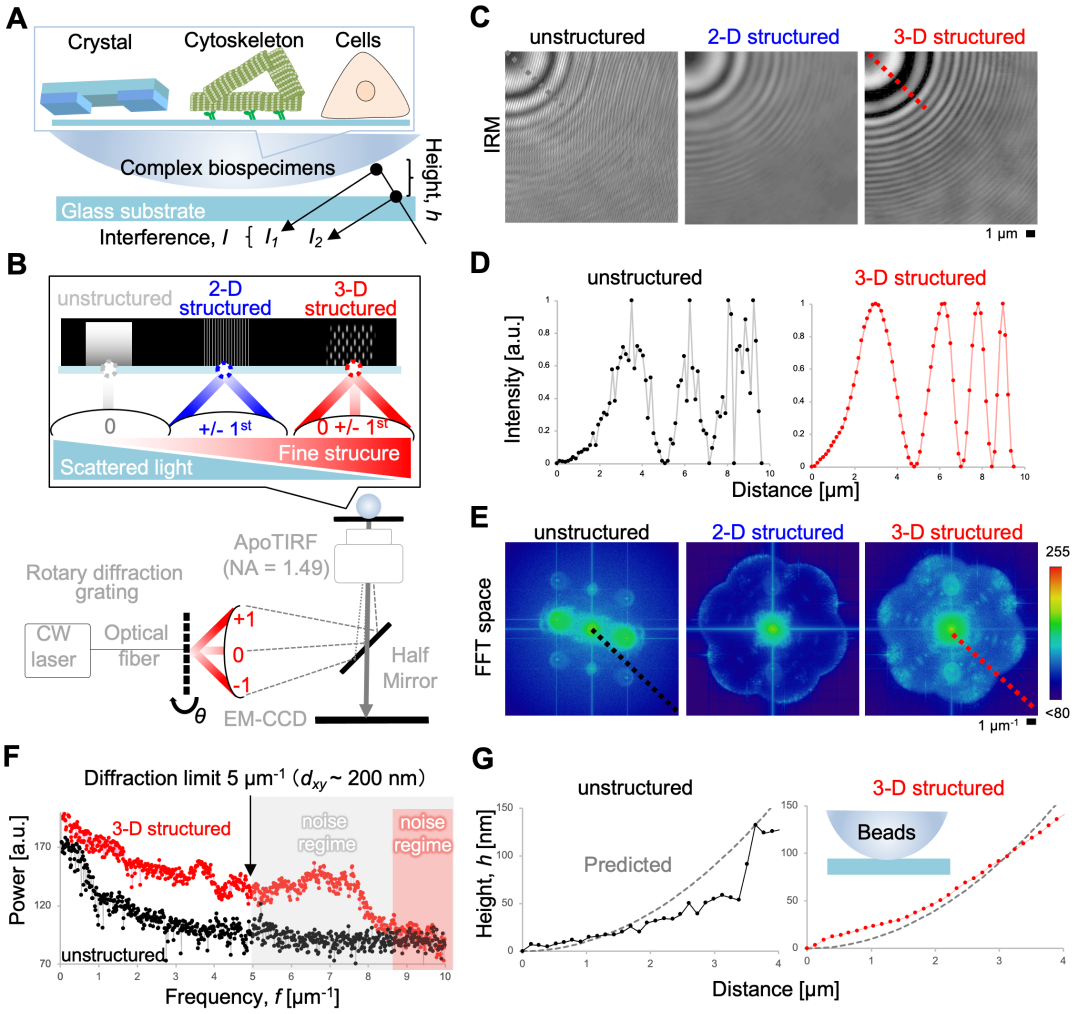


**Figure 1: 3-D structured illumination enhances the image contrast, and IRM's theoretical basis for height reconstruction remains.** (A) Concept of 3-D SIM-IRM for visualizing the surface fine structure of complex biospecimens. Principles of visualizing biospecimens-substrate height ($h$) via interference between $I_1$ and $I_2$. (B) Optical setup, and schematics of prepared structured illumination. A CW laser combined with rotary diffraction grating provides laterally (2-D) and axially (3-D) aligned Moiré patterns, reducing multiple-scattered reflections from biospecimens. (C) IRM images of a polystyrene bead (diameter, $\varphi$ = 100 μm) on a glass substrate under un/2-D/3-D structured illuminations ($\lambda$ = 488 nm) and corresponding (D) intensity profiles according to the dotted line in C. (E) Calculated FFT images from C and (F) power spectrum according to the dotted line in E. (G) Reconstructed height profiles from D using Eq 2. The predicted height profile of a spherical bead is displayed as a gray line.

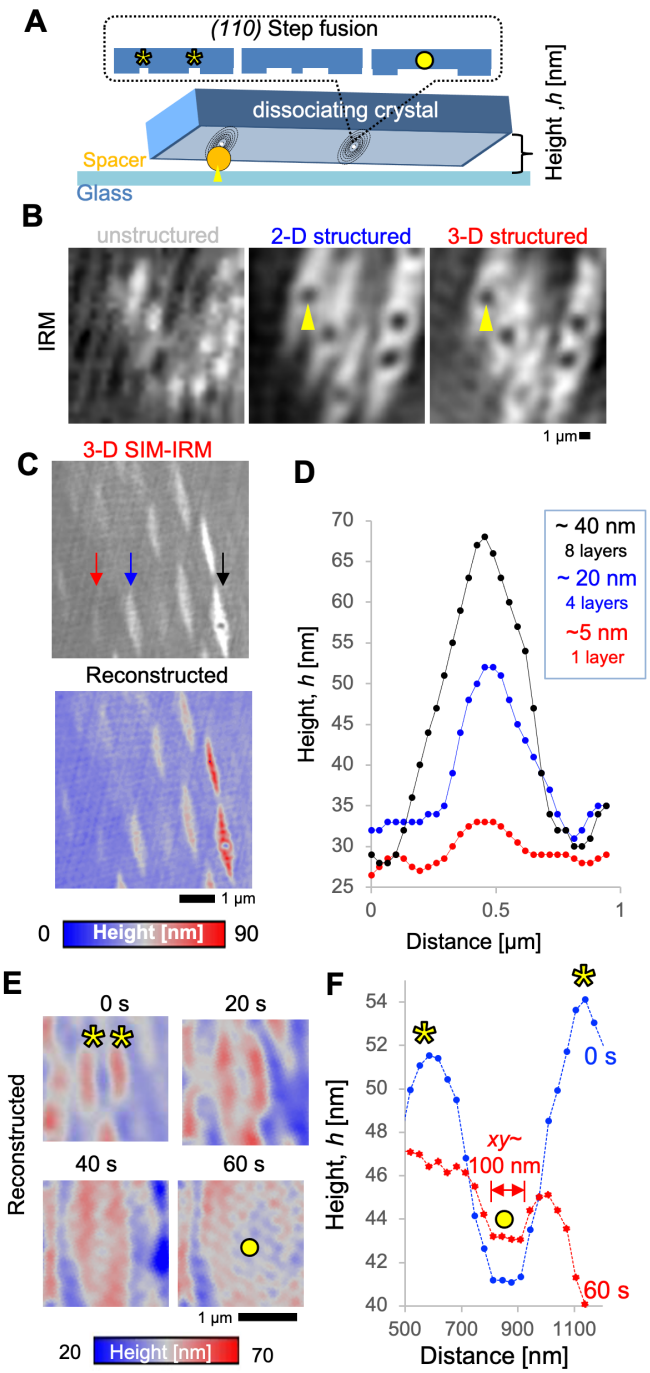


**Figure 2: Elementary step-scale visualization of the dissolution dynamics of lysozyme crystal on (110) surface.** Experimental setup for observing lysozyme-substrate height. Silica beads (φ = 100 nm) were used as spacers (yellow arrowhead). (B) IRM images during crystal dissolution under un/2-D/3-D structured illumination (λ = 488 nm). (C) A 3-D SIM-IRM image of dissolving crystals and its reconstructed height images. (D) Height profiles along the etch pit in C: red (single layer of protein molecule), blue (4 layers), and black (8 layers). (E) Timelapse of height change in dissolving crystal and its (F) topological profiles across etch pits. Adjacent pits ($h$ ~ 10 nm, $t$ = 0 s asterisk) fuse to form a single etch pit ($t$ = 60 s, circle) with a fine structure ($xy$ ~ 100 nm, $z$ ~ 2 nm).

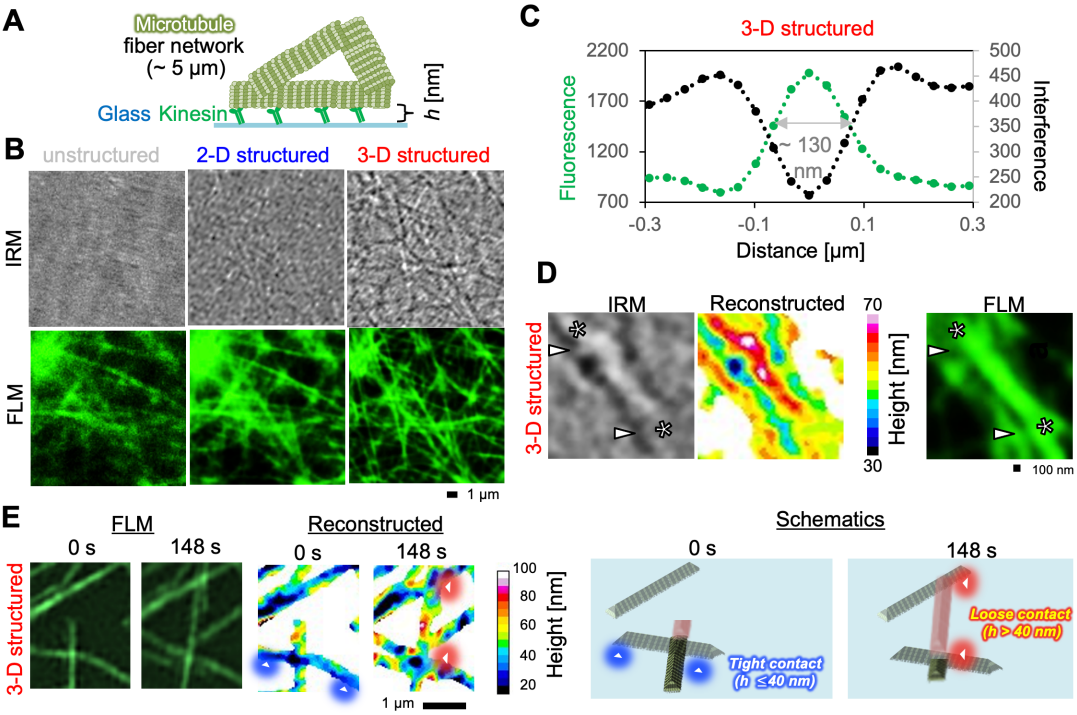


**Figure 3: Not 2-D but 3-D SIM-IRM visualized complex microtubule fiber networks unveiling adhesion dynamics along the optical axis.** (A) Experimental setup for preparing a microtubule network on the glass substrate. Motor protein (kinesin) drives the locomotion of the network by adding ATP. (B) IRM and FLM (fluorescence microscope) images of the networks under un/2-D-/3-D-structured illumination (λ = 488 nm (IRM), λ = 561 nm (FLM)). (C) Representative intensity profiles across the microtubule fiber in the network. The full width at half maximum (FWHM) is approximately 130 nm, which is beyond the diffraction limit of conventional IRM. (D) Images of 3-D SIM-IRM, its reconstructed height, and 3-D SIM-FLM of the microtubule fiber networks. Different interference intensities originate from height, *h* from the underlying substrate (close: arrowhead, farther: asterisk) (E) Timelapse of 3-D SIM-FLM images, reconstructed height images from 3-D SIM-IRM images, and its schematics of the locomoting networks in the presence of ATP. An increase in height (red arrowhead) is beyond the diameter of a microtubule fiber[26]; thus the fibers locomote onto the fibers.

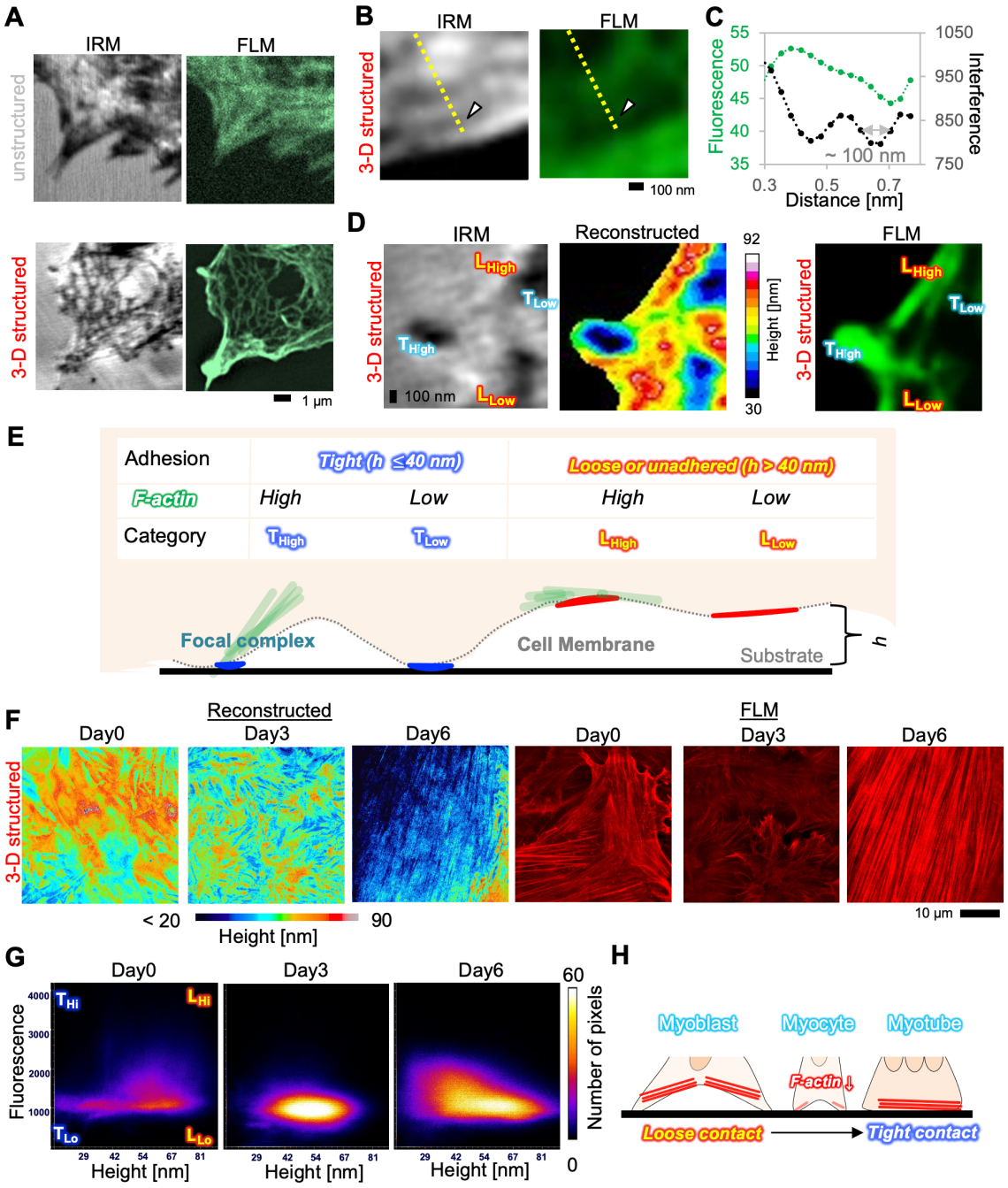


**Figure 4: Simultaneous interference/fluorescence imaging of membrane/cytoskeleton structures classified the local distribution of fine adhesion structures, and detected adhesion transition during myogenic differentiation.** (A) IRM and FLM images of different myoblasts expressing fluorescent F-actin under un/3-D- structured illumination (λ = 488 nm (IRM), λ = 561 nm (FLM)). (B) Magnification of 3-D SIM-IRM/-FLM images and (C) corresponding intensity profiles according to the dotted lines in B. FWHM of dark fibrous structure (arrowhead) in an IRM image showed approximately 100 nm, which is beyond the diffraction limit ($d_{xy}$ ~ 200 nm). (D) 3-D SIM-IRM, reconstructed height, and 3-D SIM-FLM images of myoblast. Here, the adhesion's structure is first classified into tight contact ($T_{High}$ and $T_{Low}$) and loose contact (or unadhered, $L_{High}$ and $L_{Low}$) at the threshold $h$ ~ 40 nm, which is the comparable size of the cell adhesion molecules[17]. Then, the structure of cell adhesion can be further classified according to the higher fluorescent ($T_{High}$ and $L_{High}$) and lower fluorescent ($T_{Low}$ and $L_{Low}$) of *F*-actin. (E) Schematic illustration of spatial and axial structures at cell membrane of D. (F) Timelapse of reconstructed height and 3-D SIM-FLM images of myoblasts during myogenic differentiation from myoblast (Day 0), myocyte (Day 3) to myotubes (Day

6). Low serum medium activates cellular fusion from Day 4 (**Figure S4A**). (G) Colocalization plots between fluorescence intensity and height of each pixel from F. The spatial size of each dot corresponds to the nano-scale adhesion structure (~ 30 × 30 nm) with the classification according to the categories in E. (H) Schematics of the change in cell adhesion structure during differentiation. The narrowing of plot distribution (Day 3) and peak shift toward the region of $T_{High}$ (Day 6) in G supports the new physical marker for myogenic differentiation.